The EMBO Journal (2011) 30, 1841–1851 | © 2011 European Molecular Biology Organization | All Rights Reserved 0261-4189/11
www.embojournal.org

THE EMBO JOURNAL

Transcriptome asymmetry within mouse zygotes but not between early embryonic sister blastomeres

Matthew D VerMilyea[1,6], Matthias Maneck[2,3,6], Naoko Yoshida[1,4], Isabell Blochberger[2], Emi Suzuki[1], Toru Suzuki[1,5], Rainer Spang[3], Christoph A Klein[2,7,*] and Anthony CF Perry[1,5,7,*]

[1]Laboratory of Mammalian Molecular Embryology, RIKEN Center for Developmental Biology, Kobe, Japan, [2]Department of Pathology, University of Regensburg, Regensburg, Germany, [3]Institute of Functional Genomics, University of Regensburg, Regensburg, Germany, [4]Department of Biomedical Sciences, Ritsumeikan University, Shiga, Japan and [5]Department of Biology and Biochemistry, Laboratory of Mammalian Molecular Embryology, and Bath Centre for Regenerative Medicine, University of Bath, Bath, UK

Transcriptome regionalization is an essential polarity determinant among metazoans, directing embryonic axis formation during normal development. Although conservation of this principle in mammals is assumed, recent evidence is conflicting and it is not known whether transcriptome asymmetries exist within unfertilized mammalian eggs or between the respective cleavage products of early embryonic divisions. We here address this by comparing transcriptome profiles of paired single cells and sub-cellular structures obtained microsurgically from mouse oocytes and totipotent embryos. Paired microsurgical spindle and remnant samples from unfertilized metaphase II oocytes possessed distinguishable profiles. Fertilization produces a totipotent 1-cell embryo (zygote) and associated spindle-enriched second polar body whose paired profiles also differed, reflecting spindle transcript enrichment. However, there was no programmed transcriptome asymmetry between sister cells within 2- or 3-cell embryos. Accordingly, there is transcriptome asymmetry within mouse oocytes, but not between the sister blastomeres of early embryos. This work places constraints on pre-patterning in mammals and provides documentation correlating potency changes and transcriptome partitioning at the single-cell level.
The EMBO Journal (2011) **30,** 1841–1851. doi:10.1038/emboj.2011.92; Published online 5 April 2011
Subject Categories: RNA; development
Keywords: mouse metaphase II; polarity; pre-implantation embryo; pre-patterning; transcriptome

*Corresponding authors. CA Klein, Department of Pathology, University of Regensburg, Franz-Josef-Strauß-Allee 11, 93053 Regensburg, Germany. Tel.: +49 941 944 6720; Fax: +49 941 944 6719; E-mail: christoph.klein@klinik.uni-regensburg.de or ACF Perry, Department of Biology and Biochemistry, Laboratory of Mammalian Molecular Embryology, Bath Centre for Regenerative Medicine, University of Bath, Bath BA2 7AY, UK. Tel.: +44 1225 386 936; Fax: +44 1225 386 779; E-mail: perry135@aol.com
[6]These authors contributed equally to this work
[7]Cosenior authors

Received: 3 December 2010; accepted: 3 March 2011; published online: 5 April 2011

Introduction

Fertilization naturally transforms two highly differentiated gamete cells—sperm and egg—into a single, totipotent cell that gives rise to a complete individual. This represents the most radical programmed change in cellular potency, from assured cell death if the gametes do not combine, to the establishment of a totipotent embryo if they do. The cell fate shift that occurs during fertilization may be archetypal and promises to provide insights into diverse changes of cellular potency.

Cellular potency is in some cases regulated by controlling the asymmetric distribution of cell fate determinants during division, so that each daughter cell receives a distinctive complement that contributes to a corresponding lineage commitment (Macara and Mili, 2008). This mechanism operates in stem cells, which can divide to produce one daughter cell with conserved stem cell characteristics and a second daughter cell committed to differentiation (Lin, 2008). For example, *Drosophila* neuroblasts inherit basolateral-apical polarity and harbour a spindle aligned along this axis; division is perpendicular to the axis and produces a daughter neuroblast that inherits apical determinants, and what becomes a ganglion mother cell (Chia *et al*, 2008). Cleavage asymmetry is determined by the apical localization of two complexes linked by Inscuteable (Insc) that ensure eccentric positioning of the spindle; one includes Bazooka-Par3, aPKC and Par6 and another contains Gαi, Partner of Insc (Pins) and Locomotion defect (Loco) (Cai *et al*, 2003; Lee *et al*, 2006; Chia *et al*, 2008). In *Caenorhabditis elegans*, phosphorylated LGL protein facilitates embryonic polarity by localizing the Par3–Par6–aPKC complex to an anterior cortical domain (Hoege *et al*, 2010). In mammalian skin stratification and differentiation, the Par3–LGN–Inscuteable complex and NuMA-dynactin orient the spindle perpendicularly to the basement membrane, generating a committed suprabasal cell and a proliferative basal progenitor cell (Lechler and Fuchs, 2005). These and other precedents imply that many features underlying asymmetric cell division are conserved between species and tissues (Macara and Mili, 2008).

The asymmetric localization of cytoplasmic mRNAs is a conserved evolutionary strategy by which cell polarity is regulated (Macara and Mili, 2008), although its direct contribution to the establishment of pluripotency and asymmetric stem cell division is poorly understood. By contrast, it is well documented that the targeted localization of cytoplasmic mRNAs is a key mechanism by which asymmetric patterning is achieved in metazoan oocytes and early totipotent embryos that establish stem cell lineages (Rebagliati *et al*, 1985; Melton, 1987; Lécuyer *et al*, 2007; Macara and Mili, 2008; Holt and Bullock, 2009). In *Drosophila*, at least 10% of the oocyte transcriptome is distributed non-uniformly (Dubowy and MacDonald, 1998) and the value rises to 71% in early embryos (Lécuyer *et al*, 2007). Vertebrates such as

Xenopus laevis localize synthesis of maternal (oocyte) proteins by compartmentalizing mRNAs (King, 1995; Mowry and Cote, 1999; King *et al*, 2005; Holt and Bullock, 2009). This is critical for the specification of embryonic animal and vegetal poles (Nieuwkoop, 1985), which requires faithful asymmetric transcript placement. For example, misplacement of the vegetal pole mRNA, *Vg1*, into the oocyte animal hemisphere induces ectopic mesoderm (Thomsen and Melton, 1993) and injection of *xBic-C* mRNA in whole embryos leads to ectopic endoderm formation (Wessely and De Robertis, 2000).

Oocyte localization of some *Xenopus* vegetal mRNAs involves mitochondrial clustering (Balbiani body formation) during maturation (Heasman *et al*, 1984; Kloc *et al*, 1996). Maturing mouse oocytes also possess a Balbiani body, suggesting that mechanisms involving asymmetry have been conserved (Pepling *et al*, 2007; Kloc *et al*, 2008), but although asymmetric mRNA distribution occurs in some mammalian cell types (Landry *et al*, 1994; Mili *et al*, 2008), it is unknown whether it does in mammalian oocytes and early embryos.

This issue is central to whether or not oocyte and/or early embryo patterning affects the establishment of totipotency in mammalian development, with arguments both for (Piotrowska *et al*, 2001; Plusa *et al*, 2005) and against (Hiiragi and Solter, 2004; Motosugi *et al*, 2006; Kurotaki *et al*, 2007). Levels of H3 dimethylated on arginine 26 (H3R26me2) and H3R17me2 correlated in the blastomeres of 4-cell mouse embryos with the subsequent fate of each blastomere lineage; H3R26me2 levels were lowest in blastomeres predominantly contributing to the trophectoderm (TE) and highest in blastomeres contributing more cells to the inner cell mass (ICM) and juxtaposed polar TE (Torres-Padilla *et al*, 2007). Methyl groups are transferred to residues that include H3R26 by the Carm1 methylase to promote asymmetric divisions (Schurter *et al*, 2001; Torres-Padilla *et al*, 2007; Parfitt and Zernicka-Goetz, 2010). Blastomeres with higher Carm1 levels exhibit reduced expression of Par3 and increased expression of PKCII, a truncated version of aPKCζ (Parfitt and Zernicka-Goetz, 2010). These findings are consistent with the transcriptomic asymmetries in early *Xenopus* embryos. Apparently contrary data supporting an ontogeny of early embryonic lineages that is not pre-determined maternally or in the earliest phase of embryogenesis (Kurotaki *et al*, 2007) are also consistent with models in which pre-patterning naturally primes blastomeres for ICM specification and nearest neighbour induction (Supplementary Figure S1).

In the mouse, totipotency (the natural ability of a cell to yield, through successive divisions, an entire individual) is established soon after fertilization in the 1-cell embryo and persists until the 8-cell stage (Tarkowski, 1959; Kelly, 1977). To address whether asymmetric mRNA sorting in early embryos might account for developmental polarity during the establishment and maintenance of the totipotent state, we determined transcriptome distributions within mouse oocytes and pre-nuclear zygotes (before pro-nucleus formation), and between the sister blastomeres of single embryos following first (1-cell→2-cell) and second (2-cell→3-cell) mitotic divisions. Transcriptome asymmetries exist in mouse oocytes and pre-nuclear zygotes, but not between sister blastomeres in 2- and 3-cell embryos.

Results

Transcriptome regionalization within metaphase II oocytes

We took as our starting point mouse metaphase II (mII) oocytes since they represent a mammalian counterpart of fertilizable *Xenopus* eggs and are primed for the acquisition of totipotency. Cortical samples that contained the spindle were microsurgically removed from 10 mII oocytes to generate paired membrane-intact spindle and enucleated oocyte samples (Figure 1A). Transcriptomes from each spindle sample and its matched enucleated oocyte remnant (referred to as spindle–oocyte couplets) were independently amplified (Hartmann and Klein, 2006) and subjected to microarray analysis (Supplementary Table S1). We screened for transcripts with an average spindle enrichment or depletion compared with levels in their matching enucleated oocyte counterparts, using linear models in a paired test scenario (Smyth, 2004). After adjusting *P*-values for multiple testing (Benjamini *et al*, 2001), 95 transcripts remained with significantly higher abundance in the spindle sample and 289 with significantly lower abundance (Supplementary Table S1). Microarray data were in good (83.3%) directional agreement with ratiometric quantitative PCR (qPCR) analysis of 30 transcripts in independently isolated single spindle–oocyte couplets (Figure 1B; Supplementary Table S2).

We investigated whether individual spindle samples could be identified from a characteristic transcript profile by adapting shrunken centroid classification (Tibshirani *et al*, 2002) and applying it to the paired profile scenario. For each profile pair, one profile was selected at random (i.e., the spindle sample or its associated oocyte remnant) and the value for each transcript was subtracted from the corresponding value in the matched profile. We then trained a shrunken centroid classifier to predict whether each difference profile was of the spindle–oocyte or oocyte–spindle type, in effect training the classifier to identify the profile of the spindle sample in each profile pair. The classifier did not produce any misclassifications in 10-fold cross-validation (Figure 1C). This suggests that programmed sorting of mRNAs produces characteristic and distinguishable transcriptomes in spindle and oocyte remnant samples. Analysis by qPCR revealed differences in relative levels of selected mRNAs between spindle-containing and other cortical regions (Figures 1D–F).

Distinct second polar body and zygote transcriptomes

We next investigated whether oocyte intracellular asymmetry was preserved in the pre-nuclear zygote immediately after fertilization. The second polar body (Pb_2) is produced by asymmetric cytokinesis ∼2 h after sperm–egg fusion (∼10 h before major zygotic transcription; Aoki *et al*, 1997) and contains ∼4.5% of the zygote volume (∼12 versus 268 pl) and one maternal chromosome set and spindle half. Formation of the Pb_2 after fertilization can be regarded as a non-invasive cytoplasmic sampling of the zygote from which it is derived. Immediately after Pb_2 extrusion following fertilization *in vitro*, Pb_2–zygote couplets, representing 16 embryos, were separated (Figure 2A) and their transcriptomes independently amplified and subjected to microarray analysis (Hartmann and Klein, 2006). Employing the same supervised machine learning approach described above for spindle–oocyte couplets, we were able to separate Pb_2s from zygotes with a cross-validation

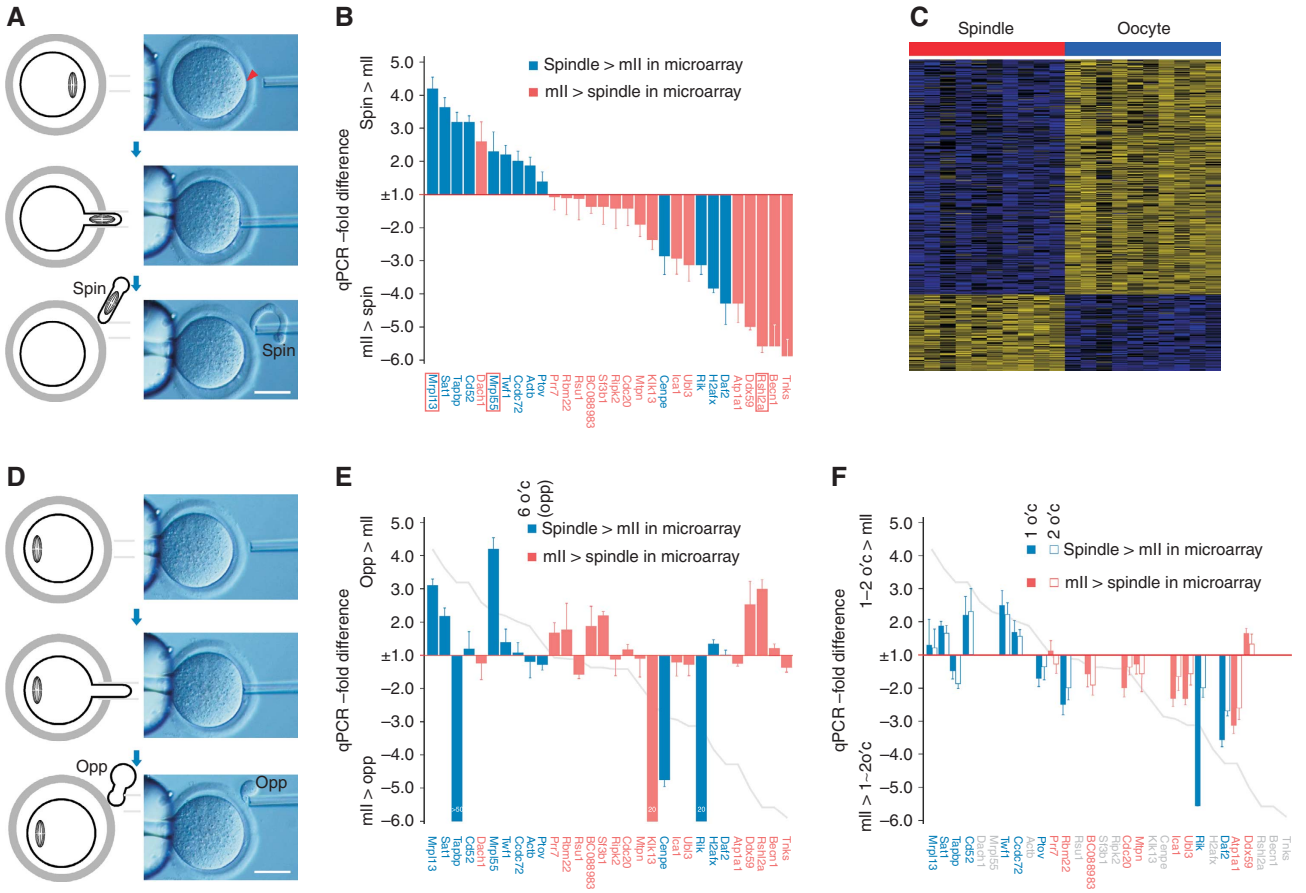

Figure 1 Sub-cellular analysis of mII oocyte transcriptomes. (**A**) Hofmann images showing microsurgical mII oocyte spindle cortex sampling. The procedure does not cause plasma membrane breakage. (**B**) Comparative qPCR analysis of spindle–oocyte couplets, shown as −fold change in spindle RQ values relative to those of the oocyte. RQ values were normalized against *H3f3a* (Supplementary Figure S5). (**C**) Heat map representing the 384 transcripts detected at significantly different levels between spindle samples and their matching mII oocyte remnants. (**D**) Hofmann images showing microsurgical cortical sampling opposite (opp) the mII oocyte spindle (i.e., at 180°, or 6 o'clock, to the spindle). (**E**) Comparative qPCR analysis as per (**B**) (grey line plot) except that cortical samples were obtained from opposite the spindle. (**F**) Comparative qPCR analysis as per (**B**) (grey line plot) in which cortical sampling was at ∼30° (1 o'clock, 1 o'c) or ∼60° (2 o'clock, 2 o'c) to the metaphase plate. In (**B**, **E** and **F**), transcripts more abundant in the spindle by microarray analysis (+ve logFC; Supplementary Table S1) are shown in blue, and those more abundant in the enucleated mII oocyte remnant in pink. Bars in (**A**, **D**) = 50 μm.

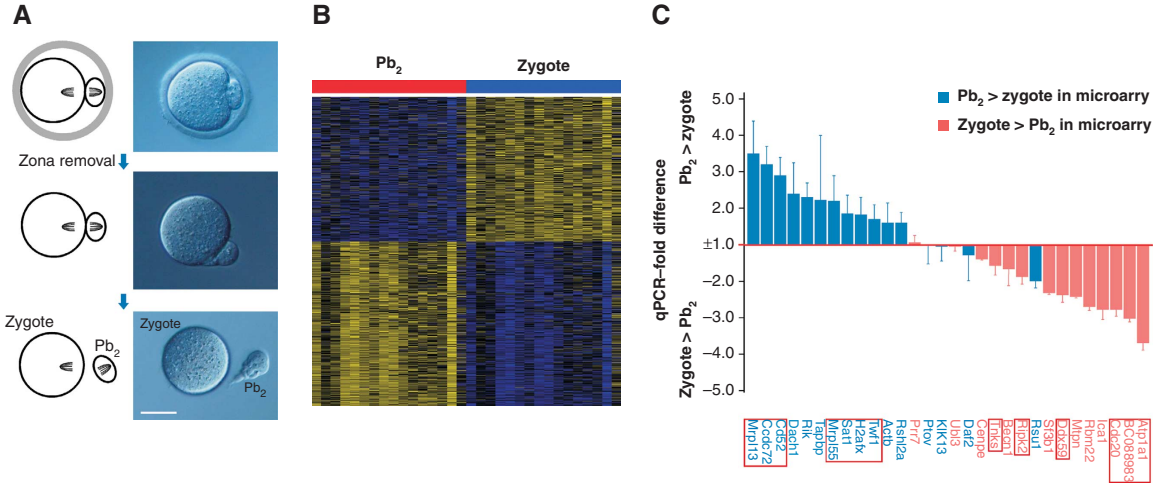

Figure 2 Transcriptome analysis of individual Pb_2–zygote couplets. (**A**) Hofmann images showing the separation of the Pb_2 from its associated zygote ∼2.5 h post-fertilization. Bar = 50 μm. (**B**) Heat map representing the 1069 transcripts that were significantly enriched or depleted in the Pb_2 relative to matching zygotes. (**C**) Comparative qPCR analysis of Pb_2–zygote couplets, shown as −fold change in Pb_2 RQ values relative to those of the zygote, normalized as per Figure 1B. Transcripts shown by microarray analysis to be more abundant in the Pb_2 (+ve logFC; Supplementary Table S3) are shown in blue, and those more abundant in the zygote in pink. Transcripts with adjusted *P*-values of <0.05 after analysis of microarray data (Supplementary Table S3) are boxed.

error of 0.0625 (1/16 couplets) (Figure 2B; Supplementary Table S3). In a gene-by-gene differential gene expression analysis, we identified 572 transcripts significantly enriched in Pb_2 samples and 497 transcripts depleted in them (Figure 2B; Supplementary Table S3). Microarray data were corroborated by qPCR analysis of independently isolated Pb_2–zygote couplets (Figure 2C; Supplementary Table S4); transcripts significantly ($P_{adj} < 0.05$) enriched in the Pb_2 were more abundant in the Pb_2 as judged by qPCR, and *vice versa* for mRNAs enriched in the zygote (Supplementary Tables S3 and S4). Thus, independent approaches indicate reproducible differences between Pb_2 and zygote transcriptome profiles.

Given that the spindle and Pb_2 are derived from the same intracellular region, their transcript contents should overlap. When the ordered lists of differentially partitioned transcripts from both experiments were compared (Lottaz *et al*, 2006), the top ends (i.e., transcripts enriched in either Pb_2 or spindle) overlapped more strongly than would have been expected by chance alone (Supplementary Figure S2; Supplementary Table S5). Compared with Pb_2–zygote pairs, fewer transcripts achieved significant concentration changes in spindle–oocyte couplets. Nevertheless, transcript rankings correlate strongly, even when including transcripts falling below the significance threshold in gene-by-gene differential gene expression analysis (Supplementary Figure S2).

Spindle- and Pb_2-enriched transcripts

Mouse orthologues of mitotic microtubular transcripts (Blower *et al*, 2007) were not differentially partitioned between Pb_2 and zygote (Supplementary Table S6) and with the sole exception (out of 19) of *Lef1* (*Tcf-1*), neither were the putative counterparts of *Xenopus* oocyte polar transcripts (Supplementary Tables S7 and S8) (King *et al*, 2005; Jambhekar and Derisi, 2007). Some asymmetrically distributed *Xenopus* oocyte transcripts are enriched ~50-fold in the vegetal pole (Mosquera *et al*, 1993), but qPCR of mouse samples did not reveal enrichment of this magnitude even among mRNAs most likely to be differentially partitioned (Figure 2C). Of 53 transcripts that are abundant during mouse oocyte maturation (Wang *et al*, 2004), 8 (15.1%) segregated significantly, 7 of these (87.5%) preferentially into the zygote (Supplementary Table S9). The pluripotency factor and marker of TE–ICM differentiation, *Sall4* (Yang *et al*, 2008; Guo *et al*, 2010) was also significantly retained by the zygote (Supplementary Table S10). Transcripts for mitochondrial ribosomal proteins L13 (*Mrpl13*) and L55 (*Mrpl55*) segregated preferentially into the Pb_2 (Figure 2C; Supplementary Table S3), but there was no accompanying expulsion of mitochondria into the Pb_1 during oocyte maturation *in vitro* (data not shown), and if anything, mitochondria were excluded from the Pb_2 as judged by video microscopy and qPCR (Supplementary Figures S3A and B). Based on the few reports of asymmetric mouse oocyte components (Antczak and Van Blerkom, 1997; Ninomiya and Ichinose, 2007), we found no indication that *Stat3*, *Lep* or 16S mitochondrial RNAs were asymmetrically sorted between Pb_2 and zygote (Supplementary Figure S3C).

Gene ontology (GO) analysis revealed that the Pb_2 was enriched for transcripts encoding negative transcriptional regulators and Ca^{2+} binding and transport activities (Table I). The zygote retained mRNAs involved in the cell cycle and lipid biosynthesis, which behave characteristically during early development (Shoji *et al*, 2006; Comiskey and Warner, 2007), and intracellular organelles, consistent with the early embryonic function of, and mRNA retention by the endoplasmic reticulum (Macara and Mili, 2008). The retention of mRNAs encoding Zn^{2+}-binding proteins may reflect recently appreciated roles for Zn^{2+} during meiosis and the induction of embryogenesis (Suzuki *et al*, 2010a, b).

No programmed transcriptome partitioning between 2-cell blastomeres

We next addressed whether the non-uniform spatial transcript distribution in oocytes and zygotes is transmitted to the early embryo such that sister blastomere products of the first mitosis inherit distinct transcriptomes, as they do in *Xenopus* early embryos (King *et al*, 2005).

To this end, transcriptome profiles were determined and statistically compared for sister blastomeres that had been separated within ~10 min of the first mitotic (1-cell→2-cell) division (Figure 3A). This comparison is not supervised as it had been in spindle–oocyte and Pb_2–zygote analyses. Even assuming that each 2-cell embryo consisted of one cell with an 'A-type' transcriptome and a second cell with a 'B-type' transcriptome, it is not, *a priori*, possible to assign a given cell to a given cell type. However, in this hypothetical scenario, if

Table I Gene ontology (GO) analysis of enriched transcripts

Enrichment	GO term	GO ID (*P*)	Rel
Pb_2	Transcription regulator activity^{mf}	0030528 (0.006)	5
	Negative regulation of transcription^{bp}	0016481 (0.005)	29
	Calcium ion binding^{mf}	0005509 (0.039)	2
	Calcium ion transport^{bp}	0006816 (0.038)	4
Zygote	Transcription coactivator activity^{mf}	0003713 (0.007)	3
	Transcription factor complex^{cc}	0005667 (0.036)	12
	zinc ion binding^{mf}	0008270 (0.043)	2
	Mesoderm development^{bp}	0007498 (0.022)	6
	Acyltransferase activity^{mf}	0008415 (0.003)	3
	Lipid biosynthetic process^{bp}	0008610 (0.0005)	11
	Cell cycle^{bp}	0007049 (0.038)	2
	Reproductive process in a multicellular organism^{bp}	0048609 (0.029)	5
	Endoplasmic reticulum membrane^{cc}	0005789 (0.002)	16

GO analysis of transcripts enriched in the second polar body (Pb_2) or zygote remnant (zygote) of Pb_2–zygote couplets (Supplementary Table S3). Additional related terms ('Rel'; $P < 0.05$) contain ⩾50% identical Entrez gene Ids, respectively, in the same enrichment and GO abbreviation categories: 'mf', molecular function; 'bp', biological process; 'cc', cellular component.

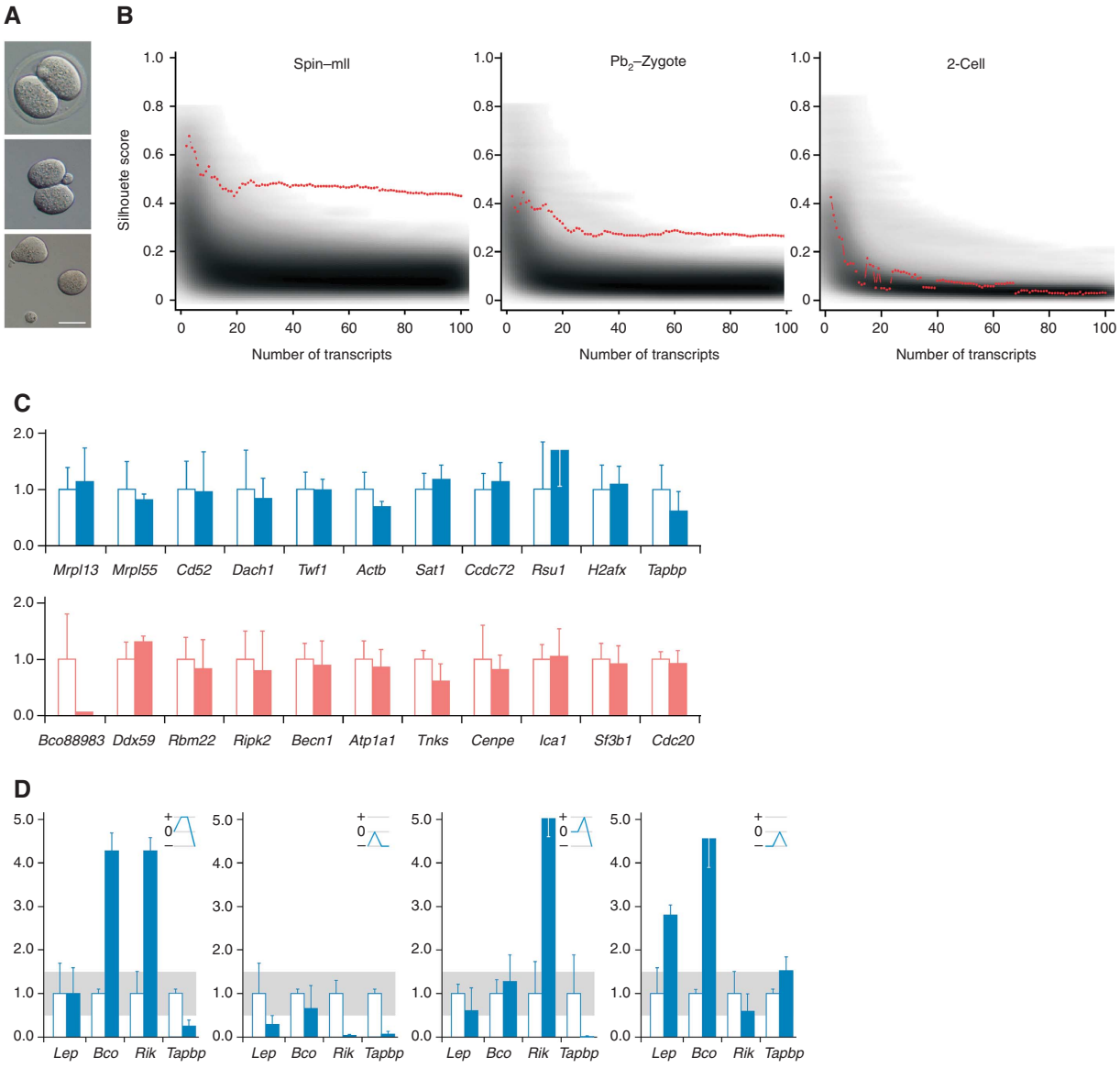

Figure 3 No programmed transcriptome sorting between 2-cell embryo sister blastomeres. (**A**) Two-cell embryo (top) blastomere separation (Hofmann) showing zona removal (centre) and separated blastomeres. Bar = 50 μm. (**B**) Clustering analysis. Red lines display separation strengths (*y* axis) of a clustering using the top *N* separating transcripts (*x* axis). Grey background shading indicates the distribution of matching random separation strengths. Sub-plots show analyses of spindle–oocyte remnants (left), Pb_2–zygote couplets (centre) and 2-cell blastomeres (right). (**C**) qPCR analysis of 2-cell blastomeres for transcripts as per Figure 1B. The value for one randomly selected blastomere is shown relative to that of its sister, set at 1.00. (**D**) Levels of the transcripts that differed most between 2-cell blastomeres were co-determined in the same four 2-cell embryos (numbered 1–4) as per Figure 1B. Blue lines in upper right hand panels represent expression level changes; small changes (0.5–1.5, grey band) are represented as 0, and an increase or decrease as + or −, respectively. No given profile is superimposable on any other or its reciprocal, which is inconsistent with co-segregation of the transcripts analysed.

one of the cells could be assigned to the 'A-type' the other would have to be of the 'B-type', distinguishing the situation from standard unsupervised learning problems. To address this and to harness the paired profile structure of the data, we developed an analysis strategy based on the significance of separation strength across multiple clusters. For every transcript in each matched pair of sister blastomere profiles, the mean abundance value of a given transcript was subtracted from both individual abundance values, such that if a transcript had a 'centred abundance' of x in one of the cells it necessarily had a 'centred abundance' of $-x$ in its sister cell. We next ranked transcripts by regularized one-sample *t*-scores (Tusher *et al*, 2001) and discarded all but the top *N* transcripts from the analysis. Finally, the centred *N* transcript profiles were clustered into two groups to generate potential 'A-type' and 'B-type' groups. Clustering was performed by the robust 'partitioning around medoids' algorithm (Kaufman and Rousseeuw, 2005). Both centring and transcript selection introduced weak but detectable cluster-like structure into the data where no such structure existed before these pre-processing steps, and this effect was enhanced when the number of selected transcripts was small (data not shown). A larger number of transcripts, *N*, faded the cluster structure, since transcriptome asymmetries do not affect all transcripts.

We varied *N* between 2 and 100 transcripts and compared the separation strengths of clusters measured by silhouette

scores (Rousseeuw, 1987) as a function of the number of selected transcripts *N* observed in the blastomere data, with the distribution of cluster strengths resulting only from the pre-processing steps on 10 000 sets of randomly selected transcripts. However, the observed cluster strengths were similar to those of random clusters (Figure 3B). We thus conclude that there is no detectable difference between the transcriptomes of sister cells in 2-cell embryos. In contrast, the same analysis strategy applied to spindle–oocyte and Pb_2–zygote sample data (Figure 3B), produced separation strengths exceeding chance expectation and confirming spindle–oocyte and Pb_2–zygote assignments. This validates our approach and shows that the analysis strategy has the power to uncover hidden classes of transcriptomes.

Consistent with these analyses, we were unable to classify 2-cell blastomeres by qPCR; blastomeres from a given couplet typically possessed similar specified mRNA levels (Figure 3C). Of these, the largest differences detected did not co-segregate; blue-line profiles were neither superimposable nor reciprocal (Figure 3D). In sum, this evidence supports the idea that non-uniform transcript distribution within zygotes does not manifest itself as unequal transcript segregation between the blastomeres of 2-cell mouse embryos.

Second mitotic products lack programmed transcriptome asymmetry

Indiscriminate transcriptome segregation between 2-cell embryonic blastomeres does not formally exclude the possibility that transcriptome asymmetry within each 2-cell blastomere leads to programmed asymmetric transcriptome inheritance following second mitotic (2-cell→3-cell and 3-cell→4-cell) divisions, to generate asymmetry between sister cells (Figure 4A). To evaluate this possibility, we generated transcript profiles for the individual blastomeres of 3-cell embryos (triplet blastomeres). Real-time movies revealed an average lag between 2-cell→3-cell and 3-cell→4-cell divisions of 75.5 ± 22.1 min ($n = 21$), placing an approximate upper limit for time elapsed since the 2-cell→3-cell division.

The 3-cell scenario yields constraints that need to be reflected in statistical analysis. Given that the first mitotic division does not alter the transcriptomic complement, an hypothetical asymmetric second mitotic division would generate transcript abundances for which the abundance in the first mitotic product of the triplet embryo is lower than that of one of the second mitotic products and higher than that of the other. We subtracted the transcript abundance of the first division cell ('a' in Figures 4A and B) from all other abundance levels including that of the second division cell ('b' and 'β' in Figures 4A and B), resulting in a constant 'centred abundance' of 0 for the entire a-profile and 'centred abundances' that can in general be either positive or negative in b- and β-profiles. The assumption of a symmetric first division followed by a second asymmetric division raises the expectation that we obtain one positive and one negative value in matched b- and β-profiles. The non-parametric Jonckheere–Terpstra test (*jt*-score) (Jonckheere, 1954) aims at detecting this data pattern. As in the case of the 2-cell blastomere analysis, we selected the top *N* most informative genes, now using the *jt*-score, and proceeded with clustering the 'centred' *N* transcript profiles. However, cluster separation strengths did not exceed random expectations (Figure 4C). Moreover, when 12 of the original 30 transcripts (Figure 1B) were tested by qPCR, they were similarly apportioned between second mitotic products (cells b and β), corroborating the microarray analysis (Figure 4D). Thus, we found no evidence for programmed transcriptome asymmetry between the sister blastomeres of 3-cell embryos.

Discussion

We here report single sub-cellular profiling to reveal intracellular mRNA regionalization on a transcriptome-wide level. This is perhaps the first time that the transcriptomes of nascent cleavage products of mammalian cells have been determined and compared to determine whether programmed asymmetries exist between each. Because the experiments were performed in a standardized model of shifted cellular potency, they have implications for the underlying mechanisms. They are consistent with a role for non-uniform mRNA sorting as a prelude to the establishment of totipotency, and have implications for pre-patterning in mouse embryos, in which two distinct lineages differing in phenotype, position and fate first appear at the 8–16-cell morula stage (Ducibella and Anderson, 1975; Johnson and Ziomek, 1981; Guo *et al*, 2010).

The question as to when mammalian pre-implantation embryonic lineages are first specified has produced contradictory conclusions. One view holds that 2-cell blastomeres cannot be classified according to reproducible differences between them; neither makes a biased contribution to the ICM or TE (Hiiragi and Solter, 2004; Motosugi *et al*., 2005; Kurotaki *et al*, 2007; Guo *et al*, 2010). This model is corroborated by 'real-time' analyses of pre-implantation development showing that 2-cell blastomeres do not differ in their contribution to the ICM or TE (Kurotaki *et al*, 2007). However, this finding is consistent with a model in which pre-patterning does occur and promotes coordinated specification of the 'ICM lineage' during normal development (Supplementary Figure S1) and is predicated on the finding that the blastomeres of 4-cell embryos differ epigenetically (Piotrowska and Zernicka-Goetz, 2001; Piotrowska *et al*, 2001; Plusa *et al*, 2002, 2005; Torres-Padilla *et al*, 2007; Parfitt and Zernicka-Goetz, 2010).

Programmed transcriptome differences between sister blastomeres at the 4-cell stage (which in the mouse are totipotent; Kelly, 1977) could in principal adopt what is a broadly employed mechanism (Macara and Mili, 2008) to ensure differential patterning between the blastomeres, but we found no evidence of this. In addition, we found no evidence for pre-disposing transcriptome asymmetry between the blastomeres of 2-cell embryos or non-uniform sorting of *Carm1* ($P = 0.532$), *Par3* (*Pard3*, $P = 0.143$) or *aPKCζ* (*Prkcz*, $P = 0.850$) transcripts in pre-nuclear zygotes (Supplementary Table S3). These observations would seem to argue against targeted mRNA localization as a means of allocating lineage fate in totipotent mouse embryos in that they suggest that any transcriptomic pre-patterning during the first two mitotic divisions is either too subtle for detection thus far or non-existent. As such, if there is maternal or early embryonic patterning in mammals, it is more likely to be mediated post-translationally. This is in marked contrast to the pronounced, targeted localization of oocyte-derived mRNAs in *Drosophila* and *Xenopus*, which result in

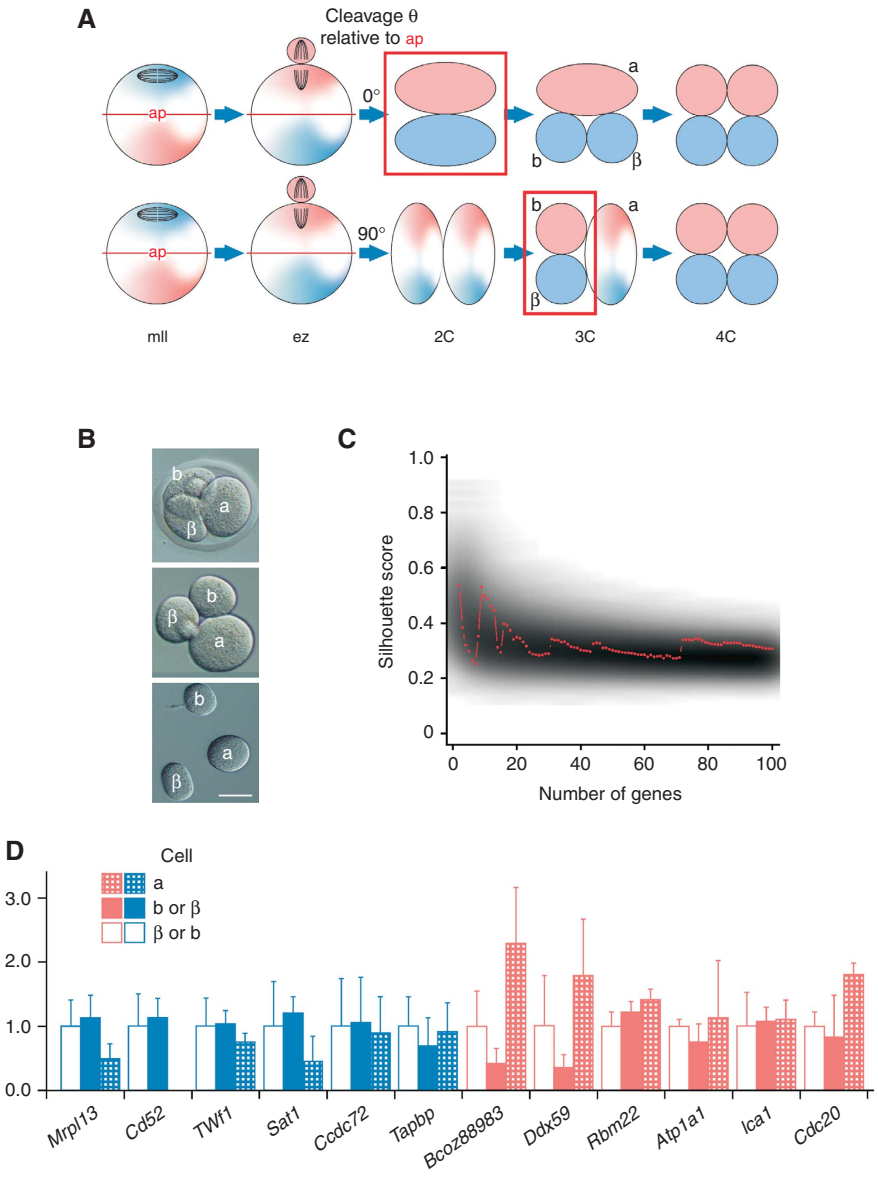

Figure 4 No asymmetric transcriptome sorting between 3-cell embryo sister blastomeres. (**A**) Asymmetric maternal transcriptome inheritance may persist through the early zygote (ez) and not be detected until the first (upper) or second mitotic division. Polarity determinants marking two lineages are shown as pink or blue. Asymmetry detection (boxed) is possible after first (upper) or second mitoses. First (a) and second (b and β) mitotic products are shown; ap, asymmetry plane. (**B**) Three-cell embryo (top) blastomere separation (Hofmann) showing zona removal (centre) and separated blastomeres <15 min after 2-cell→3-cell division. Bar = 50 μm. (**C**) Clustering analysis. Red line displays separation strengths (*y* axis) of a clustering using the top *N* separating transcripts (*x* axis). Grey background shading indicates the distribution of matching random separation strengths. (**D**) Comparative qPCR analysis of 3-cell blastomeres for transcripts as per Figure 1B. The value for one of the second mitotic blastomeres (b, labelled as per (**A**) and (**B**)) is set at 1.0, shown relative to values for the first mitotic (2-cell) blastomere (a) and the sister second mitotic blastomere (β).

developmentally critical transcriptome partitioning between embryonic cells (King *et al*, 2005; Blower *et al*, 2007; Lécuyer *et al*, 2007).

It remains to be seen why the mouse does not utilize a developmental mechanism that is so highly conserved and why there is transcriptome asymmetry within mouse oocytes. It is possible that the asymmetry reflects benign carryover from earlier oocyte development, during which mRNA localization had a critical role. Spindle complexes are sites of targeted polysomal mRNA localization in diverse systems (Blower *et al*, 2007; Mili and Macara, 2009) and spindles characteristically orchestrate key elements of mouse oocyte maturation (Brunet and Verlhac, 2011). Spindle enrichment of mRNAs might thus localize translation to target proteins during the establishment of a fertilizable mII oocyte. Of the many processes that may be regulated in this manner, candidates include modulators of the cell cycle (e.g., Emi2), spindle-dependent remodelling (e.g., Ran GTPase) and asymmetric cytokinesis (e.g., Par6) (Vinot *et al*, 2004; Dumont *et al*, 2007; Suzuki *et al*, 2010a).

Alternatively, the programmed ejection of transcripts into the Pb_2 may provide a unique tier of gene regulation during the gamete-to-embryo transition. However, the elimination of Pb_2 components is not critical in the mouse; replacing the

zygotic female pro-nucleus with a nucleus derived from the Pb_2 following electrofusion of the entire Pb_2 supports full development to term (Wakayama *et al*, 1997). While this work precludes an essential developmental role for Pb_2–zygote transcriptome partitioning, taken with our data, it is entirely consistent with such sorting exerting non-absolute effects for normal rates of healthy mammalian development. Given this, the Pb_2 signature transcriptome might serve to inform strategies for RNA-induced pluripotent stem cell generation (Warren *et al*, 2010) and as a diagnostic tool by providing markers of embryo viability, enabling single embryo selection in human assisted reproduction (Brison *et al*, 2007).

Materials and methods

A summary diagram showing relationships between samples is shown in Supplementary Figure S4.

Animal care

Experiments were performed in accordance with local and national statutes protecting animal welfare in experimental research.

Collection and culture of mII oocytes

Oviductal mII oocytes were typically collected from 8- to 12-week-old $B6D2F_1$ females supplied by SLC (Shizuoka-ken, Japan) 12–15 h after standard superovulation (by serial equine and human chorionic gonadotropin injection, eCG and hCG) and cumulus cells removed following hyaluronidase treatment as previously described (Yoshida *et al*, 2007). All oocyte and embryo culture was in humidified CO_2 (5% (v/v) in air) at 37°C as previously described (Yoshida *et al*, 2007).

Collection of Pb_2–zygote couplets following in vitro fertilization (IVF)

Embryos for the preparation of nascent zygote–Pb_2 couplets were generated by standard $B6D2F_1 \times B6D2F_1$ IVF. Sperm were collected from mature males by epididymidal puncture followed by dispersal for 5 min in pre-warmed human tubal fluid (HTF; ARK Resource Co. Ltd., Japan) in humidified CO_2 (5% (v/v) in air) at 37°C. A drop (10 μl of the 400 μl dispersal droplet) was transferred to a fresh, fertilization dish containing 200 μl HTF and incubation continued for 1 h before placing ~30 cumulus oophorous complexes freshly isolated from superovulated 8-week-old $B6D2F_1$ females and continuing the incubation for further 2–3 h. Complexes were chosen whose oocytes did not have an extant Pb_1 to assist with identification of Pb_2 extrusion and reduce contamination with mRNA from earlier stages. Following incubation, each pre-nuclear zygote (i.e., preceding the formation of pro-nuclei) was briefly treated with acid Tyrode's solution (Sigma) on a stage heated to 37°C (to remove its zona pellucida) and then subjected to gentle pipetting (pipette aperture ≈250 μm) to separate the Pb_2 from its coupled zygote. The resultant Pb_2 and zygote were immediately and separately transferred either to 5 μl mTRAP™ (Active Motif, Carlsbad, CA) (for microarray analysis) or to 1 μl Sarkosyl (Teknova, Hollister, CA) (for real-time, semi-quantitative PCR, qPCR) containing 10 ng/ml tRNA (Roche, Mannheim) and flash-frozen in liquid nitrogen and stored at −80°C in preparation for cDNA synthesis.

To confirm spindle separation following cytokinesis, Pb_2–zygote couplets were stained by incubating in Hoechst 33342 (Sigma, 2.5 μg/ml) in M2 medium at room temperature for 10 min. Stained couplets were washed in fresh M2 medium and transferred to fresh M2 medium for fluorescence imaging using a BioZero-8000 microscope/detector (Keyence, Osaka, Japan) and analysed with BZ-Analyzer software (Keyence).

Collection of blastomeres from 2- and 3-cell embryos

Oviductal embryos were removed from plugged, superovulated 8-week-old $B6D2F_1$ females 0.5–1.5 days after they had been mated with $B6D2F_1$ males for 2- and 3-cell embryo collection as follows. For 2-cell embryo collection, zygotes (1-cell) were harvested 22–24 h post-hCG (the afternoon after mating) and following cursory cumulus cell removal, and incubated in batches of 5–10 per culture dish in KSOM medium (Yoshida *et al*, 2007). Under these conditions, first mitotic cleavage (to produce 2-cell embryos) could be monitored every ~10 min with minimal disturbance to other embryos and typically occurred within 1 h of culture. Cleavage was therefore identified within ~10 min. Newly formed 2-cell embryos were removed into acid Tyrode's solution to remove the zona pellucida as for Pb_2–zygote separation. Embryos were then washed twice in CZBH medium (Chatot *et al*, 1989) and subjected to gentle pipetting (pipette aperture ≈250 μm). This generally separated sister blastomeres within 1 min. Separated blastomeres were immediately and separately transferred either to 5 μl mTRAP (Active Motif) (for microarray analysis) or to 1 μl Sarkosyl (Teknova) (for qPCR) containing 10 ng/ml tRNA (Roche), flash-frozen in liquid nitrogen, and where necessary stored at −80°C.

For the separation of 3-cell embryo blastomeres, 2-cell embryos were collected ~46 h post-hCG and incubated in M2 medium (humidified CO_2, 37°C) in batches of 5–10 as described above. This allowed us to monitor cleavage and catch 3-cell embryos before the 3-cell→4-cell division. Three-cell embryos were subjected to acid Tyrode's treatment and gentle pipetting to separate blastomeres as described above, except that trituration was typically in Ca^{2+}-free CZBH (Chatot *et al*, 1989). Sister blastomeres (second mitotic products) were clearly distinguishable from the larger avuncular blastomere (first mitotic product) (Figure 4B). The 2-cell→3-cell cleavage was typically identified within ~15 min of its having occurred. Separated blastomeres were transferred either to 5 μl mTRAP or to 1 μl Sarkosyl containing 10 ng/ml tRNA (as per 2-cell embryo blastomeres), flash-frozen in liquid nitrogen and stored at −80°C.

Microsurgery

Microsurgery (Yoshida and Perry, 2007) was performed on oocytes collected 12–14 h post-hCG and within 16 h of hCG administration unless stated otherwise. We used the hybrid strain, $B6D2F_1$, in which the position of the mII spindle is clearly discernable because of the pronounced cortical bump it produces (Yoshida and Perry, 2007). Piezo-actuated microsurgery of oocytes was in CZBH supplemented with 5 μg/ml cytochalasin B on a 37°C heated stage, essentially as described (Yoshida and Perry, 2007; Yoshida *et al*, 2007) and was always completed within 3 min. Pipette tip inner diameters were of 7–8 μm. These procedures did not generally result in oocyte plasma membrane breakage. Although the spindle position is plainly discernable in $B6D2F_1$ mII oocytes, spindle sampling was confirmed in two ways. First, expulsion from the pipette of samples containing spindles produces an elongated 'sausage', whereas cortical samples lacking spindle material are rotund (Figure 1D). This characteristic appearance confirmed in all cases that the spindle had been harvested where that was the intention. Second, DNA staining of microdissected spindle samples and their paired enucleated oocytes confirmed that spindles were consistently removed in their entirety ($n = 52$). Intact plasma membranes typically encapsulated spindle-containing and other cortical samples. Immediately after microdissection, samples in minimum extraneous media (<0.5 μl) were separately drawn into a pipette (aperture ≈250 μm) and bubbled either into 5 μl mTRAP (Active Motif) containing 10 ng/ml tRNA and stored at −80°C for microarray analysis or into 1 μl Sarkosyl (Teknova) containing 10 ng/ml tRNA for immediate cDNA synthesis, for qPCR.

Where appropriate, mII oocytes were pre-incubated in KSOM supplemented with 10 μM nocodazole (Sigma) before sampling in CZBH containing 5 μg/ml cytochalasin B plus 10 μM nocodazole. To confirm spindle sampling during nocodazole treatment, oocytes were transferred to nocodazole-containing KSOM supplemented with Hoechst 33342 (Sigma, 2.5 μg/ml), 30 min before microsurgery. DNA was visualized by halogen lamp illumination and this enabled confirmation of chromatin removal.

Ratiometric PCR (qPCR)

For ratiometric transcript quantification in single cells and cell fragments, total RNA was extracted by transferring them in a minimal volume (<0.5 μl) into 1 μl 0.1% (w/v) Sarkosyl (Teknova) containing 10 ng/ml tRNA (Hoffmann-La Roche Ltd., Basel, Ch), heated at 65°C for 5 min and used to programme cDNA synthesis primed with oligo$(dT)_{20}$ and random 8-mers (each at 30 μM) in a 21-μl reaction volume containing 200 U SuperScript III reverse transcriptase (Invitrogen Corp., Carlsbad, CA). Where multiple

samples were collected serially in the same time frame (<2 h), they were stored on ice and processed in parallel starting with heating at 65°C. Real-time qPCR was in an ABI 7500 Real Time PCR System (Applied Biosystems, Foster City, CA) in reactions (20 μl total) containing 1–2 μl of the template cDNA, forward and reverse primers (Supplementary Table S11; 100 nM each) and 12.5 μl of Power SYBR (ABI), using the parameters: 10 min at 95 °C, followed by 45 cycles of 15 s at 95°C, 1 min at 58–60°C and 35 s at 72°C. Primer sets (Hokkaido System Science, Hokkaido, Japan) yielded 111–186 bp products were typically intron flanking and non-dimerizing under the conditions employed. Where oocytes or embryos failed to produce amplimers, primer efficacy was confirmed using testis- and/or brain-derived cDNA. Reverse transcriptase minus reactions were used to verify absence of contamination in cocktail components. Steady-state levels of transcripts were normalized with respect to the internal reference, *H3f3a* (May *et al*, 2009). *H3f3a* was preferred to other commonly used standards because it was sufficiently abundant for detection in sub-cellular samples while exhibiting minimal cross-sample variation (Supplementary Figure S5). Reactions were performed in triplicate and fold changes calculated by dividing the mean for one sample by the mean of its coupled sample. Fold changes in Figures 1 and 2 and Supplementary Figure S3 were calculated by dividing the means for samples with smaller volumes (e.g., spindles in Figure 1 and Pb_2s in Figure 2) by the means of their corresponding larger couplets (oocyte remnants in Figure 1 and zygotes in Figure 2). Where values for means were smaller than 1, reciprocal values were calculated to show a fold decrease but bars show original values for standard errors. Note that the dynamic range of qPCR is known to be greater than that of microarrays; they produce similar directions, but not necessarily magnitudes, of transcript level differences between samples (Park *et al*, 2004; Hartmann and Klein, 2006).

PCR for microarray analysis

Total RNA from single cells or sub-cellular fragments was extracted and uniformly amplified essentially as previously described (Hartmann and Klein, 2006). Single cells and sub-cellular fragments isolated by micromanipulation in 5 μl lysis buffer (Active Motif, Rixensart, Belgium) containing 10 ng tRNA (Roche) were supplemented with 1 μg protease (Active Motif), 1 μl biotinylated oligo-dT peptide nucleic acids (PNAs) (Midi-Kit, Active Motif, dissolved in 400 μl of water). Proteolytic digestion was at 45°C for 10 min, followed by 1 min at 75°C and 15 min at 22°C for PNA annealing. Isolation of mRNA was with 4 μl streptavidin beads (Active Motif) during 45 min rotation at room temperature. Wash buffer 1 (10 μl; 75 mM KCl, 10 mM DTT and 0.25% Igepal, 50 mM Tris-Cl; pH 8.3) was added and the tubes placed into a magnetic rack. Supernatant was removed and the beads washed in wash buffer 2 (20 μl; 75 mM KCl, 10 mM DTT, 0.5% (v/v) Tween-20, 50 mM Tris–HCl; pH 8.3). Supernatant was removed and the step repeated with 20 μl cDNA wash buffer 1. Reverse transcription was performed under rotation for 45 min at 44°C in a mixture containing each dNTP at 0.5 mM, 200 U Superscript II (Invitrogen, Karlsruhe), 30 μM CFL15CN8 primer (C_{15}GTCTAGAN_8), 15 μM CFL15CT24 primer (C_{15}GTCTA GAT_{24}VN), 0.25% (v/v) Igepal, 10 mM DTT (Invitrogen) and the buffer supplied by the manufacturer in a final volume of 20 μl. Primers were annealed at room temperature for 10–15 min before addition of the enzyme. Following reverse transcription, beads were washed in 20 μl tailing wash buffer (50 mM KH_2PO_4, 1 mM DTT, 0.25% (v/v) Igepal; pH 7.0) and resuspended in 10 μl tailing buffer (10 mM KH_2PO_4, 4 mM $MgCl_2$, 0.1 mM DTT, 200 μM dGTP; pH 7.0). cDNA–mRNA hybrids were denatured at 94°C for 4 min and 10 U terminal deoxynucleotide transferase (Amersham, Freiburg) was added and incubation continued at 37°C for 60 min for G-tailing. After inactivation of the tailing enzyme (70°C, 5 min), PCR mix I (4 μl buffer 1 (Expand Long Template, Roche), 3% (v/v) deionized formamide) was added to each sample. Hotstart PCR was performed by adding 5.5 μl PCR mix II (350 μM dNTPs, 1.2 μM CP_2 primer (TCAGAATTCATGC$_{15}$) and 7.5 U Pol Mix (Expand Long Template)). Forty cycles were run in a MJ research PCR machine: 20 cycles of 15 s at 94°C, 30 s at 65°C, 2 min at 68°C and 20 cycles with an elongation of the extension time of 10 s and a final elongation step of 7 min at 68°C.

Sample labelling and array hybridization

Labelling and microarray hybridization were performed essentially as described previously (Hartmann and Klein, 2006). Primary cDNA amplification products were labelled in the presence of 3% (v/v) formamide, 2.4 μM CP2-BGL primer (TCAGAATTCATGCCGCCC CCCCGGCCC), dNTPs (0.35 mM dATP and dGTP, 0.3 mM dTTP and dCTP) and 50 μM labelled nucleotides. Sample cDNA was labelled with digoxygenin-dUTP (Roche) and aminodigoxygenin-dCTP (Perkin-Elmer, Rodgau-Jügesheim), and reference cDNA with biotin-dUTP (Roche) and biotin-dCTP (Invitrogen). Primers were removed by digestion with 30 U *Bgl*I (Fermentas, St Leon-Rot) and the samples purified on a column (Qiagen, Hilden). Murine Operon 70mer oligonucleotide arrays (Version 2) spotted on Ultra-GAPS slides (Operon, Köln resp. Corning, Schiphol-Rijk, Netherlands) were pre-hybridized with 5 × SSC, 0.1% (w/v) SDS, 0.1% (w/v) BSA at 42°C and hybridized in an Arraybooster hybstation (Implen, Munich) at 42°C overnight. Washing steps following hybridization were at 42°C twice in 2 × SSC, 0.1% (w/v) SDS for 5 min, twice in 0.5 × SSC, 0.1% (w/v) SDS for 10 min, and twice in 0.1 × SSC for 2.5 min. Non-specific binding of labelled proteins was blocked with 1% (v/v) blocking reagent for nucleic acid hybridization (Roche) followed by a staining procedure with anti-Dig-Cy5 and streptavidin-Cy3 (Jackson Laboratories) each at 16 μg/ml. Excess antibody/streptavidin was removed with 4 × SSC, 0.2% (v/v) Tween-20 and slides were scanned on a Genepix 4000A scanner (Axon Instruments, Union City).

Microarray data pre-processing

Microarray data pre-processing was performed in R using the *limma* package (Smyth and Speed, 2003). Raw probe intensities were background corrected by applying the 'normexp' method (Smyth and Speed, 2003). Analyses were restricted to cy5 intensities, since cy3 intensities did not capture fold changes correctly in spike-in experiments of single-cell expression assays (not shown). Loess normalization was used in M versus A plots of individual cy5 intensities of a given transcript in a given array and the median cy5 intensity across all arrays of the same transcript. Log2 ratios were calculated from the normalized intensities and quantile normalization was applied across arrays. All further analysis was based on normalized log ratios.

Differential expression analysis

Transcripts present at significantly different levels between groups were identified using regularized linear models as implemented in the *limma* package (Smyth, 2004). Transcripts were considered differentially expressed where their corresponding adjusted *P*-value (P_{adj}; corrected for multiple testing as proposed previously; Benjamini *et al*, 2001) was $\leqslant 0.05$. The pairing of profiles from the same couplets was performed in Pb_2 versus zygotes and spindle versus oocyte remnant comparisons. In the joint analysis of Pb_2–zygote and spindle–oocyte couplets, we aim for transcript abundances with imbalances in the Pb_2–zygote comparison and the reverse imbalance in the spindle–oocyte comparison. We tested for differences of differences, where the inner differences were, respectively, between matched Pb_2–zygote and spindle–oocyte couplets and the outer difference was between these differences. Significantly over-represented GO-Terms in the lists of differential transcript abundances between Pb_2 and zygote as well as spindle and mII oocyte were identified using Fisher's exact test. The rankings of transcript lists resulting from both comparisons were tested for significant similarity as described previously (Yang *et al*, 2006) implemented in the R package *OrderedList* (Lottaz *et al*, 2006).

Classification of paired profiles

Supervised classification analysis was performed using the shrunken centroid method (Tibshirani *et al*, 2002) as implemented in the R package, *PAMr*. Pb_2–zygote couplets were randomly sorted into two groups of equal size, A and B. For group A couplets, the zygote profile was subtracted from the Pb_2 profile transcript by transcript, while for group B couplets we reversely subtracted, Pb_2 from zygote profiles transcript by transcript. Shrunken centroid classification was used to predict whether a couplet was in group A or B. In other words, the classifier was trained to detect the zygote profile in each profile pair from a couplet. Classification accuracy was assessed in 10-fold cross-validation. The analysis of spindle versus oocyte remnants was performed in an analogous manner.

Cluster analysis of pair and triplet profiles

For every transcript and every pair of couplet profiles, the mean abundance of the transcript was subtracted from both individual abundances. Transcripts were then ranked by regularized one-sample *t*-scores (Tusher *et al*, 2001) and all but the top *N* transcripts were discarded. The resultant truncated profiles were clustered into two groups using the *Partitioning around Medoids* algorithm (Kaufman and Rousseeuw, 2005). Clustering separation strengths were measured by silhouette scores (Rousseeuw, 1987) as a function of the number of selected transcripts, *N*. The significance of cluster strengths was assessed by comparing them with cluster strengths calculated in the same way for 10 000 sets of randomly selected transcripts. For triplet data (of blastomeres immediately following the 2-cell→3-cell division), we centred each triplet around the first mitotic (1-cell→2-cell) product in the 3-cell embryo by subtracting the corresponding expression value from all profiles in the triplet. Transcripts were ranked by the Jonckheere–Terpstra test (Lehman, 1975) and all but the top *N* transcripts discarded. Resultant truncated profiles were clustered into three groups using the *Partitioning around Medoids* algorithm (Kaufman and Rousseeuw, 2005). Separation strengths were assessed and tested as for paired data.

Accession numbers

Array data are deposited at the Gene Expression omnibus (GEO). Accession number GSE27396.

Supplementary data

Supplementary data are available at *The EMBO Journal* Online (http://www.embojournal.org).

Acknowledgements

We are extremely grateful to Maki Asami for critically reading the manuscript and for grant support from RIKEN (ACFP), and the DFG (SPP1190) and the Bavarian State Ministry of Sciences, Research and the Arts (CAK).

Author contributions: MV, NY, IB, ES, TS and ACFP performed the experiments, which were designed by CAK and ACFP with input from RS. MM, RS and CAK performed data analysis. ACFP wrote the paper with additional material from RS and CAK.

Conflict of interest

The authors declare that they have no conflict of interest.

References

Antczak M, Van Blerkom J (1997) Oocyte influences on early development: the regulatory proteins leptin and STAT3 are polarized in mouse and human oocytes and differentially distributed within the cells of the preimplantation stage embryo. *Mol Hum Reprod* **3:** 1067–1086

Aoki F, Worrad DM, Schultz RM (1997) Regulation of transcriptional activity during the first and second cell cycles in the preimplantation mouse embryo. *Dev Biol* **181:** 296–307

Benjamini Y, Drai D, Elmer G, Kafkafi N, Golani I (2001) Controlling the false discovery rate in behavior genetics research. *Behav Brain Res* **125:** 279–284

Blower MD, Feric E, Weis K, Heald R (2007) Genome-wide analysis demonstrates conserved localization of messenger RNAs to mitotic microtubules. *J Cell Biol* **179:** 1365–1373

Brison DR, Hollywood K, Arnesen R, Goodacre R (2007) Predicting human embryo viability: the road to non-invasive analysis of the secretome using metabolic footprinting. *Reprod Biomed Online* **15:** 296–302

Brunet S, Verlhac MH (2011) Positioning to get out of meiosis: the asymmetry of division. *Hum Reprod Update* **17:** 68–75

Cai Y, Yu F, Lin S, Chia W, Yang X (2003) Apical complex genes control mitotic spindle geometry and relative size of daughter cells in *Drosophila* neuroblast and pI asymmetric divisions. *Cell* **112:** 51–62

Chatot CL, Ziomek CA, Bavister BD, Lewis JL, Torres I (1989) An improved culture medium supports development of random-bred 1-cell mouse embryos *in vitro*. *J Reprod Fertil* **86:** 679–688

Chia W, Somers WG, Wang H (2008) *Drosophila* neuroblast asymmetric divisions: cell cycle regulators, asymmetric protein localization, and tumorigenesis. *J Cell Biol* **180:** 267–272

Comiskey M, Warner CM (2007) Spatio-temporal localization of membrane lipid rafts in mouse oocytes and cleaving preimplantation embryos. *Dev Biol* **303:** 727–739

Dubowy J, Macdonald PM (1998) Localization of mRNAs to the oocyte is common in Drosophila ovaries. *Mech Dev* **70:** 193–195

Ducibella T, Anderson E (1975) Cell shape and membrane changes in the eight-cell mouse embryo: prerequisites for morphogenesis of the blastocyst. *Dev Biol* **47:** 45–58

Dumont J, Million K, Sunderland K, Rassinier P, Lim H, Leader B, Verlhac MH (2007) Formin-2 is required for spindle migration and for the late steps of cytokinesis in mouse oocytes. *Dev Biol* **301:** 254–265

Guo G, Huss M, Tong GQ, Wang C, Li Sun L, Clarke ND, Robson P (2010) Resolution of cell fate decisions revealed by single-cell gene expression analysis from zygote to blastocyst. *Dev Cell* **18:** 675–685

Hartmann CH, Klein CA (2006) Gene expression profiling of single cells on large-scale oligonucleotide arrays. *Nucleic Acids Res* **34:** e143

Heasman J, Quarmby J, Wylie CC (1984) The mitochondrial cloud of *Xenopus* oocytes: the source of germinal granule material. *Dev Biol* **105:** 458–469

Hiiragi T, Solter D (2004) First cleavage plane of the mouse egg is not predetermined but defined by the topology of the two apposing pronuclei. *Nature* **430:** 360–364

Hoege C, Constantinescu AT, Schwager A, Goehring NW, Kumar P, Hyman AA (2010) LGL can partition the cortex of one-cell *Caenorhabditis elegans* embryos into two domains. *Curr Biol* **20:** 1296–1303

Holt CE, Bullock SL (2009) Subcellular mRNA localization in animal cells and why it matters. *Science* **326:** 1212–1216

Jambhekar A, Derisi JL (2007) Cis-acting determinants of asymmetric, cytoplasmic RNA transport. *RNA* **13:** 625–642

Johnson MH, Ziomek CA (1981) The foundation of two distinct cell lineages within the mouse morula. *Cell* **24:** 71–80

Jonckheere AR (1954) A distribution-free k-sample test against ordered alternatives. *Biometrika* **41:** 133–145

Kaufman L, Rousseeuw PJ (2005) *Finding Groups in Data (A Introduction to Cluster Analysis)*. Wiley: Series in Probability and Statistics 1. Edition May 2005

Kelly SJ (1977) Studies of the developmental potential of 4- and 8-cell stage mouse blastomeres. *J Exp Zool* **200:** 365–376

King ML (1995) mRNA localization during frog oogenesis. In *Localized RNAs*, Lipshitz HD (ed) pp 137–148. Austin, TX, USA: R.G. Landes

King ML, Messitt TJ, Mowry KL (2005) Putting RNAs in the right place at the right time: RNA localization in the frog oocyte. *Biol Cell* **97:** 19–33

Kloc M, Jaglarz M, Dougherty M, Stewart MD, Nel-Themaat L, Bilinski S (2008) Mouse early oocytes are transiently polar: three-dimensional and ultrastructural analysis. *Exp Cell Res* **314:** 3245–3254

Kloc M, Larabell C, Etkin LD (1996) Elaboration of the messenger transport organizer pathway for localization of RNA to the vegetal cortex of *Xenopus* oocytes. *Dev Biol* **180:** 119–130

Kurotaki Y, Hatta K, Nakao K, Nabeshima Y, Fujimori T (2007) Blastocyst axis is specified independently of early cell lineage but aligns with the ZP shape. *Science* **316:** 719–723

Landry CF, Watson JB, Kashima T, Campagnoni AT (1994) Cellular influences on RNA sorting in neurons and glia: an *in situ* hybridization histochemical study. *Mol Brain Res* **27:** 1–11

Lechler T, Fuchs E (2005) Asymmetric cell divisions promote stratification and differentiation of mammalian skin. *Nature* **437:** 275–280

Lécuyer E, Yoshida H, Parthasarathy N, Alm C, Babak T, Cerovina T, Hughes R, Tomancak P, Krause HM (2007) Global analysis of mRNA localization reveals a prominent role in organizing cellular architecture and function. *Cell* **131:** 174–187

Lee CY, Robinson KJ, Doe CQ (2006) Lgl, Pins and aPKC regulate neuroblast self-renewal versus differentiation. *Nature* **439:** 594–598

Lehman EH (1975) *Nonparametrics: Statistical Methods Based on Ranks*. p 233. San Francisco, USA: Holden Day

Lin H (2008) Cell biology of stem cells: an enigma of asymmetry and self-renewal. *J Cell Biol* **180:** 257–260

Lottaz C, Yang X, Scheid S, Spang R (2006) OrderedList—a bioconductor package for detecting similarity in ordered gene lists. *Bioinformatics* **22:** 2315–2316

Macara IG, Mili S (2008) Polarity and differential inheritance—universal attributes of life? *Cell* **135:** 801–812

May A, Kirchner R, Müller H, Hartmann P, El Hajj N, Tresch A, Zechner U, Mann W, Haaf T (2009) Multiplex RT–PCR expression analysis of developmentally important genes in individual mouse preimplantation embryos and blastomeres. *Biol Reprod* **80:** 194–202

Melton DA (1987) Translocation of a localized maternal mRNA to the vegetal pole of *Xenopus* oocytes. *Nature* **328:** 80–82

Mili S, Macara IG (2009) RNA localization and polarity: from A(PC) to Z(BP). *Trends Cell Biol* **19:** 156–164

Mili S, Moissoglu K, Macara IG (2008) Genome-wide screen reveals APC-associated RNAs enriched in cell protrusions. *Nature* **453:** 115–119

Mosquera L, Forristall C, Zhou Y, King ML (1993) A mRNA localized to the vegetal cortex of *Xenopus* oocytes encodes a protein with a nanos-like zinc finger domain. *Development* **117:** 377–386

Motosugi N, Bauer T, Polanski Z, Solter D, Hiiragi T (2005) Polarity of the mouse embryo is established at blastocyst and is not prepatterned. *Genes Dev* **19:** 1081–1092

Mowry KL, Cote CA (1999) RNA sorting in *Xenopus* oocytes and embryos. *FASEB J* **13:** 435–445

Motosugi N, Dietrich JE, Polanski Z, Solter D, Hiiragi T (2006) Space asymmetry directs preferential sperm entry in the absence of polarity in the mouse oocyte. *PLoS Biol* **4:** e135

Nieuwkoop PD (1985) Inductive interactions in early amphibian development and their general nature. *J Embryol Exp Morphol* **89** (Suppl)**:** 333–347

Ninomiya Y, Ichinose S (2007) Subcellular distribution of mitochondrial ribosomal RNA in the mouse oocyte and zygote. *PLoS ONE* **2:** e1241

Parfitt DE, Zernicka-Goetz M (2010) Epigenetic modification affecting expression of cell polarity and cell fate genes to regulate lineage specification in the early mouse embryo. *Mol Biol Cell* **21:** 2649–2660

Park PJ, Cao YA, Lee SY, Kim JW, Chang MS, Hart R, Choi S (2004) Current issues for DNA microarrays: platform comparison, double linear amplification, and universal RNA reference. *J Biotechnol* **112:** 225–245

Pepling ME, Wilhelm JE, O'Hara AL, Gephardt GW, Spradling AC (2007) Mouse oocytes within germ cell cysts and primordial follicles contain a Balbiani body. *Proc Natl Acad Sci USA* **104:** 187–192

Piotrowska K, Wianny F, Pedersen RA, Zernicka-Goetz M (2001) Blastomeres arising from the first cleavage division have distinguishable fates in normal mouse development. *Development* **128:** 3739–3748

Piotrowska K, Zernicka-Goetz M (2001) Role for sperm in spatial patterning of the early mouse embryo. *Nature* **409:** 517–521

Plusa B, Hadjantonakis AK, Gray D, Piotrowska-Nitsche K, Jedrusik A, Papaioannou VE, Glover DM, Zernicka-Goetz M (2005) The first cleavage of the mouse zygote predicts the blastocyst axis. *Nature* **434:** 391–395

Plusa B, Piotrowska K, Zernicka-Goetz M (2002) Sperm entry position provides a surface marker for the first cleavage plane of the mouse zygote. *Genesis* **32:** 193–198

Rebagliati MR, Weeks DL, Harvey RP, Melton DA (1985) Identification and cloning of localized maternal RNAs from *Xenopus* eggs. *Cell* **42:** 769–777

Rousseeuw PJ (1987) Silhouettes: a graphical aid to the interpretation and validation of cluster analysis. *J Comp Appl Math* **20:** 53–65

Schurter BT, Koh SS, Chen D, Bunick GJ, Harp JM, Hanson BL, Henschen-Edman A, Mackay DR, Stallcup MR, Aswad DW (2001) Methylation of histone H3 by coactivator-associated arginine methyltransferase 1. *Biochemistry* **40:** 5747–5756

Shoji S, Yoshida N, Amanai M, Ohgishi M, Fukui T, Fujimoto S, Nakano Y, Kajikawa E, Perry ACF (2006) Mammalian Emi2 mediates cytostatic arrest and transduces the signal for meiotic exit *via* Cdc20. *EMBO J* **25:** 834–845

Smyth GK, Speed TP (2003) Normalization of cDNA microarray data. *Methods* **31:** 265–273

Smyth GK (2004) Linear models and empirical Bayes methods for assessing differential expression in microarray experiments. *Stat Appl Genet Mol Biol* **3**: Article 3

Suzuki T, Suzuki E, Yoshida N, Kubo A, Li H, Okuda E, Amanai M, Perry ACF (2010a) Mouse Emi2 as a distinctive regulatory hub in second meiotic metaphase. *Development* **137:** 3281–3291

Suzuki T, Yoshida N, Suzuki E, Okuda E, Perry ACF (2010b) Full-term mouse development by abolishing Zn^{2+}-dependent metaphase II arrest without Ca^{2+} release. *Development* **137:** 2659–2669

Tarkowski AK (1959) Experiments on the development of isolated blastomeres of mouse eggs. *Nature* **184:** 1286–1287

Tibshirani R, Hastie T, Narasimhan B, Chu G (2002) Diagnosis of multiple cancer types by shrunken centroids of gene expression. *Proc Natl Acad Sci USA* **99:** 6567–6572

Thomsen GH, Melton DA (1993) Processed Vg1 protein is an axial mesoderm inducer in *Xenopus*. *Cell* **74:** 433–441

Torres-Padilla ME, Parfitt DE, Kouzarides T, Zernicka-Goetz M (2007) Histone arginine methylation regulates pluripotency in the early mouse embryo. *Nature* **445:** 214–218

Tusher VG, Tibshirani R, Chu G (2001) Significance analysis of microarrays applied to the ionizing radiation response. *Proc Natl Acad Sci USA* **98:** 5116–5121

Vinot S, Le T, Maro B, Louvet-Vallee S (2004) Two PAR6 proteins become asymmetrically localized during establishment of polarity in mouse oocytes. *Curr Biol* **14:** 520–525

Wakayama T, Hayashi Y, Ogura A (1997) Participation of the female pronucleus derived from the second polar body in full embryonic development of mice. *J Reprod Fertil* **110:** 263–266

Wang QT, Piotrowska K, Ciemerych MA, Milenkovic L, Scott MP, Davis RW, Zernicka-Goetz M (2004) A genome-wide study of gene activity reveals developmental signaling pathways in the preimplantation mouse embryo. *Dev Cell* **6:** 133–144

Warren L, Manos PD, Ahfeldt T, Loh YH, Li H, Lau F, Ebina W, Mandal PK, Smith ZD, Meissner A, Daley GQ, Brack AS, Collins JJ, Cowan C, Schlaeger TM, Rossi DJ (2010) Highly efficient reprogramming to pluripotency and directed differentiation of human cells with synthetic modified mRNA. *Cell Stem Cell* **7:** 618–630

Wessely O, De Robertis EM (2000) The *Xenopus* homologue of Bicaudal-C is a localized maternal mRNA that can induce endoderm formation. *Development* **127:** 2053–2062

Yang J, Chai L, Fowles TC, Alipio Z, Xu D, Fink LM, Ward DC, Ma Y (2008) Genome-wide analysis reveals Sall4 to be a major regulator of pluripotency in murine-embryonic stem cells. *Proc Natl Acad Sci USA* **105:** 19756–19761

Yang X, Bentink S, Scheid S, Spang R (2006) Similarities of ordered gene lists. *J Bioinform Comp Biol* **4:** 693–708

Yoshida N, Amanai M, Fukui T, Kajikawa E, Brahmajosyula M, Iwahori A, Nakano Y, Shoji S, Diebold J, Hessel H, Huss R, Perry AC (2007) Broad, ectopic expression of the sperm protein PLCZ1 induces parthenogenesis and ovarian tumours in mice. *Development* **134:** 3941–3952

Yoshida N, Perry ACF (2007) Piezo-actuated mouse intracytoplasmic sperm injection (ICSI). *Nat Protoc* **2:** 296–304